

# Coupled Dipole Calculation of Extinction Coefficient and Polarization Ratio for Smoke Agglomerates

GEORGE W. MULHOLLAND and RAYMOND D. MOUNTAIN

National Institute of Standards and Technology, Gaithersburg, MD 20899 USA

The mass specific extinction coefficient and the polarization ratio at 90° of simulated smoke agglomerates are computed for clusters with 3 to 1390 primary spheres and for size parameter from 0.05 to 0.6 using the coupled electric and magnetic dipole (CEMD) method. For the size parameter range of interest for postflame smoke, the specific extinction coefficient computed by CEMD is 21% to 36% greater than Rayleigh prediction, and for this size range for clusters with 100 to 1000 primary spheres, the range in the specific extinction coefficient is about 12%. Agreement between measured and predicted specific extinction coefficient would require selection of a refractive index outside the range of values widely used by the combustion community. The polarization ratio at 90° is found to be a monotonic function of primary sphere size and relatively independent of agglomerate size. Comparison with the limited experimental results indicates potential for polarization ratio as a diagnostic for primary sphere size. © 1999 by The Combustion Institute

## INTRODUCTION

In a previous study, the light scattering characteristics of clusters made up of 2 to 165 spheres were computed using the coupled electric and magnetic dipole method (CEMD) [1]. This study focussed on comparing results with an exact solution and with a Rayleigh-Debye analysis for fixed orientations. Here we extend the treatment to include orientation averaging and larger agglomerates with up to 1390 spheres to allow comparison with other models and experiments. The primary focus of this analysis is to determine the effect of cluster size and primary sphere size on both the specific light extinction coefficient and the polarization ratio for smoke agglomerates.

### Specific Extinction Coefficient

Perhaps the most widely used measurement of smoke is the extinction coefficient  $k_e$ , which is obtained from the ratio of the transmitted to incident light intensity,  $I/I_0$ , over a pathlength,  $L$ .

$$I/I_0 = \exp(-k_e L) \quad (1)$$

The mass concentration of soot,  $m$ , is determined from  $k_e$  and the mass specific extinction coefficient  $\sigma_e^m$ ,

$$\sigma_e^m = k_e/m \quad (2)$$

The mass concentration is an important property for fire safety in terms of reduced visibility for people escaping from fire situations, the amount of thermal radiation emitted by a flame, and for environmental/climate/health effects for the smoke released from large fires into the atmosphere. The value of  $\sigma_e^m$  must be known before  $m$  can be determined from optical measurements. In general one expects  $\sigma_e^m$  to depend on the size and structure of the smoke. However, for one case the value of  $\sigma_e^m$  is independent of the size distribution. This is in the small particle limit of Mie theory for which the following expression is obtained:

$$\sigma_e^m = \frac{6\pi E(n)}{\lambda \rho_s}, \quad (3)$$

$$E(n) = +Im\left(\frac{n^2 - 1}{n^2 + 2}\right). \quad (4)$$

The quantity  $\lambda$  is the wavelength of light,  $\rho_s$  is the density of the solid phase of the smoke, and  $n$  is the complex refractive index. This result, which is valid for size parameter  $x_p < 0.1$ , is termed the Rayleigh limit.<sup>1</sup> The size parameter  $x_p$  is defined as the ratio of the particle circumference to the wavelength of light.

\*Corresponding author. E-mail: george.mulholland@nist.gov

<sup>1</sup>The expression *Rayleigh limit* is widely used for the small particle limit for light extinction even though Rayleigh's analysis was limited to light scattering by a small sphere.

TABLE 1

Literature Values of the Complex Refractive Index of Flame-generated Smoke

| Date of Publ./Ref. | $\lambda$ , nm | Refractive Index | Fuel                           |
|--------------------|----------------|------------------|--------------------------------|
| 1969 [16]          | 650            | $1.57 + i0.44$   | acetylene                      |
|                    | 650            | $1.56 + i0.52$   | propane                        |
| 1980 [15]          | 488            | $1.7 + i0.7$     | 8 $\mu\text{m}$ carbon sphere  |
| 1981 [17]          | 633            | $1.9 + i0.55$    |                                |
| 1983 [18]          | 633            | $1.7 + i0.8$     |                                |
| 1987 [19]          | 633            | $1.85 + i0.40$   | toluene                        |
|                    | 633            | $1.85 + i0.39$   | methane                        |
| 1990 [20]          | 540            | $1.77 + i0.63$   | propane, 10 mm<br>above burner |
| 1993 [21]          | 633            | $1.53 + i0.38$   | Propane                        |

The density of postflame smoke is about  $1.8 \text{ g/cm}^3$  [2, 3] with an uncertainty of less than 5%; the uncertainty in the refractive index is much greater. A recent review by Smyth and Shaddix [4] indicates that the range in refractive index measured for smoke corresponds to a range in  $\sigma_e^m$  from  $2.2 \text{ m}^2/\text{g}$  to  $4.0 \text{ m}^2/\text{g}$  for a wavelength equal to  $633 \text{ nm}$  and a density of  $1.8 \text{ g/cm}^3$ .

There have been several measurements of  $\sigma_e^m$  at  $633 \text{ nm}$  in the postflame region with values in the range  $7.5 \text{ m}^2/\text{g}$  to  $9.5 \text{ m}^2/\text{g}$  for smoke from a premixed acetylene air flame [5], from liquid hydrocarbon fuels and plastics from small-scale burns [6], and large-scale burns [7, 8]. Of these studies, the most accurately determined values are  $7.8 \text{ m}^2/\text{g} \pm 1.1 \text{ m}^2/\text{g}$  for the premixed acetylene flame [5] (incorrectly reported as  $8.0 \text{ m}^2/\text{g}$ ) and  $7.8 \text{ m}^2/\text{g}$  for crude oil smoke [6, 7]. We see that the measured values of  $\sigma_e^m$  are on the order of twice as large as the largest value computed above. Recent measurements by Wu et al. [9] at  $633 \text{ nm}$  for smoke produced by the burning of four gaseous hydrocarbon fuels are about a factor of 2 smaller and mostly in the range  $3.7 \text{ m}^2/\text{g}$  to  $5.5 \text{ m}^2/\text{g}$ . The reason for the difference is not known, and studies are in progress to make measurements using the same burner and fuel and to perform an absolute calibration of the specific extinction measurement in order to resolve the differences.

There are two limitations to applying Eq. 3 to smoke agglomerates: first, the primary sphere size must be small enough for the small particle limit to be applicable; and secondly there is no accommodation in the theory to account for the agglomerate structure of the smoke. One of the

primary objectives of this paper is to calculate the effects of the primary sphere size and agglomerate size on the specific extinction coefficient based on the CEMD method. The primary sphere size ranges from as small as  $10\text{--}20 \text{ nm}$  for in-flame methane soot [10], to  $30\text{--}50 \text{ nm}$  observed for postflame soot for a range of laboratory-scale burners including laminar diffusion flames [11, 12] and buoyant turbulent diffusion flames for a wide range of hydrocarbon fuels [13], to about  $100 \text{ nm}$  for postflame soot from large pool fires of crude oil [14] with a pan size of at least  $3 \text{ m}$ . For these largest particles the primary sphere size parameter  $x_p$  approaches  $0.6$ . A value of the size parameter approaching  $0.6$  would also occur for smaller flames when using a UV light source. One finds that Eq. 3 underestimates the Mie theory result for  $\sigma_e^m$  by  $8\%$  for  $x_p$  equal  $0.3$  and by  $20\%$  at  $x_p$  equal  $0.6$  for a refractive index equal  $1.7 + i0.7$ , which is based on light scattering measurements for a single spherical carbon particle [15]. A qualitatively similar result would be obtained for other estimates of the refractive index of smoke [16–21] (Table 1).

The observed constancy of  $\sigma_e^m$  is thought to be a result of the low fractal dimension, about  $1.8$ , for the smoke agglomerates. A fractal dimension less than  $2$  implies that most of the primary spheres making up the agglomerate are visible on a projected image with few totally blocked by spheres above or below. This lack of blockage leads to estimating the absorption as simply the absorption of one sphere times the total number of spheres. However, coupled dipole calculations [1, 22–24] indicate about a

10% increase in the absorption coefficient per particle for agglomerates with up to 600 particles for  $x_p \leq 0.25$ . This effect, which persists even for very small primary spheres, is discussed by Mulholland et al. [1]. For larger primary sphere sizes shielding becomes an important effect. For  $x_p \geq 0.4$  these studies indicate at least a 10% decrease in the absorption coefficient relative to Eq. 3 in the specific absorption for clusters with more than 100 primary units.

Farias et al. [24] included a wide range of cluster sizes up to 512 primary spheres and orientation averaging. Their method [24] includes only the electric dipole coupling between primary spheres and is quantitative for small primary sphere sizes with  $x_p$  less than about 0.25. The CEMD method, which includes both the electric and magnetic dipole coupling, is quantitative for size parameters up to at least 0.6. The calculations presented here include the widest range of any calculation for soot in terms of the number of primary spheres with up to 1390 and over the widest range in primary sphere size parameter up to 0.6. Such a range in agglomerate sizes is needed because of the wide range existing in smoke. Koylu and Faeth [13] estimate on average 95% of the agglomerates contain between 30 and 1800 primary spheres for eight hydrocarbon fuels burning as turbulent diffusion flames. Even larger agglomerates have been observed. Agglomerates visible to the eye with more than a million primary spheres have been produced by a laminar acetylene flame at high fuel flow rate [25] and also by the burning of polystyrene. So it is seen that results are needed for large agglomerates and ultimately will be needed for agglomerates larger than our largest size of 1390.

The light extinction coefficient is the sum of the light absorption coefficient and the light scattering coefficient. In the small particle limit given by Eq. 3 there is no scattering contribution to the extinction; however, the measured light scattering coefficient for smoke agglomerates has been found to be mostly in the range of 20% to 30% of the extinction coefficient for plastics, wood, rubber, and liquid fuels [26] and for gaseous hydrocarbon fuels [9] at visible wavelengths. The contribution of the light scattering to the extinction coefficient is expected to increase with an increase in the number of

primary spheres in the agglomerate for a fixed primary sphere size. So it is important to compute these optical properties for as large an agglomerate as possible.

While the mass concentration,  $m$ , is the primary quantity of interest for postflame smoke, the soot volume fraction  $\rho$  is the primary quantity of interest for in-flame measurements. Most studies of soot growth and burnout in laminar flames rely on light extinction measurements together with tomographic reconstruction to map out the soot volume fraction as a function of radial and vertical location. The dimensionless extinction coefficient,  $K_e$ , which is analogous to  $\sigma_e^m$ , is defined by

$$K_e = k_e \lambda / \rho \quad (5)$$

The coefficients  $K_e$  and  $\sigma_e^m$  are related by the following equation:

$$K_e = \sigma_e^m \lambda \rho_s \quad (6)$$

For the HeNe laser wavelength of 632.8 nm and a particle density of 1.800 g/cm<sup>3</sup> the product  $\lambda \rho_s$  equals 1.139 g/m<sup>2</sup>. So the measured value of  $\sigma_e^m$  for acetylene smoke of 7.8 m<sup>2</sup>/g corresponds to a  $K_e$  of 8.6 [5].

### Polarization Ratio

A second optical property of interest for characterizing smoke is the polarization ratio  $r_{pol}(\theta)$ , which is defined by the following equation

$$r_{pol}(\theta) = \frac{C_{hh}(\theta)}{C_{vv}(\theta)} \quad (7)$$

The scattering cross sections denoted by  $C$  depend on the state of polarization of the incident light and on any analyzer placed forward to the detector. This dependence is indicated by appending two subscripts to the cross sections: the first indicates the state of linear polarization of the incident light and the second indicates the orientation of the linear analyzer. The subscript  $v$  represents the direction perpendicular to the scattering plane and  $h$  represents the direction parallel to this plane.

The measurement of polarization ratio has been widely used for the measurement of small spherical particles with size parameter up to about 2 [27], over which range the polarization

ratio is monotonic in particle size. This method has been used for liquid aerosols with small particle size and for colloidal suspensions made up of spherical particles. There has been limited use of polarization ratio measurements for agglomerates in part because of a lack of an adequate theoretical framework for analyzing the measurements. D'Alessio [28] summarized the results of polarization ratio measurements of smoke produced by a variety of fuel chemistries and burner types and found the results to be inconsistent with predictions based on Mie theory, on Rayleigh theory both for a prolate spheroid and for a linear chain agglomerate theory. He pointed out the need for an optical model for agglomerated particles. Dobbins et al. [29] modeled the agglomerate structure as a porous sphere and were able to obtain fair agreement between the measured and predicted polarization ratio at  $90^\circ$ .

In this study we report results for a quantitative model for scattering by agglomerates capable of describing primary sphere sizes up to  $x_p$  equal 0.6. Our previous study suggested that  $r_{pol}(90^\circ)$  for the agglomerate was similar in magnitude to  $r_{pol}(90^\circ)$  for an isolated sphere, though the results were limited to three agglomerate sizes (17, 52, and 165 primary spheres). This result that  $r_{pol}(90^\circ)$  is directly related to the primary sphere size is the motivation for the more extensive analysis presented in this paper. There have been other analyses for determining primary sphere size from polarized and depolarized light scattering [30] and from a combination of light extinction and light scattering as a function of angle [31, 32], but none based on only light scattering measurements at a single angle. Here we extend this analysis to include orientation average, averaging over the acceptance angle of the detector, and a wide range of agglomerate sizes. The results will be compared with measured values of polarization ratios for which there are also primary sphere size measurements.

## CALCULATION METHODOLOGY

The Rayleigh-Debye scattering theory for agglomerates neglects multiple scattering within the agglomerate. The coupled dipole methods

treat the multiple scattering as a coupling between the dipole fields from the primary particles. The electric field arising from the  $n$ th dipole (primary sphere) affects the electric field at every other sphere and, vice versa, the field arising from every other dipole contributes to the field at the  $n$ th sphere. In the formulation used here we include the coupling of both the electric dipole and the magnetic dipole. This allows us to treat larger primary sphere sizes up to a size parameter of at least 0.6.

The basic CEMD method involves two steps. First solving the coupled equations given below for the field at each primary sphere in the agglomerate:

$$\vec{E}_i^r = \vec{E}_i^{r0} + \alpha_E \sum_{j \neq i}^N \tilde{C}_{ij} \vec{E}_j^r + \alpha_H \sum_{j \neq i}^N \tilde{F}_{ij} \vec{H}_j^r \quad (8)$$

$$\vec{H}_i^r = \vec{H}_i^{r0} + \alpha_H \sum_{j \neq i}^N \tilde{C}_{ij} \vec{H}_j^r + \alpha_E \sum_{j \neq i}^N \tilde{F}_{ij} \vec{E}_j^r \quad (9)$$

The quantities  $E_i^r$  and  $H_i^r$  are the electric and magnetic fields at the  $i$ th particle normalized by the magnitude of the incident field and  $E_i^{r0}$  and  $H_i^{r0}$  are the incident fields at the  $i$ th particle. The matrix elements  $C_{ij}$  and  $F_{ij}$  incorporate the  $r_{ij}$  dependent functions of the dipole fields. The electric and magnetic polarizabilities,  $\alpha_E$  and  $\alpha_H$ , are related to the Lorenz-Mie coefficients  $a_1$  and  $b_1$  [33] as follows:

$$\alpha_E = \frac{6\pi i a_1}{k^3} \quad (10)$$

$$\alpha_H = \frac{6\pi i b_1}{k^3} \quad (11)$$

In the original formulation of the coupled dipole method by Purcell and Pennypacker [34],  $a_1$  was approximated by the first term in the small  $x_p$  expansion. Dungey and Bohren [35] used the full expression for  $a_1$  to allow treatment of larger primary units and Eq. 11 is an obvious extension of their method to the magnetic dipole term.

Equations 8 and 9 are solved by successive approximation with the first-order estimate being the incident fields. Our convergence criterion is that the total scattered intensity at zero angle differ by less than 0.1% for two successive

approximations. This procedure converges for all the agglomerates (largest 1392) for the size parameter  $\leq 0.6$  but diverges for agglomerates larger than about 100 spheres for a size parameter greater than about 1. The equations have a solution for  $x_p \geq 1$ , but our solution method is not appropriate.

The second step is to compute the far field solutions given the local exciting field at each particle. These solutions are obtained as the  $1/r$  terms in the general expression from the dipole fields [1]. From these fields the differential scattering cross section and extinction cross section are obtained in the standard manner as shown by Mulholland et al. [1].

The extinction cross section for 2 touching spheres ( $x_p = 0.11$  and  $0.6$ ) and 17 touching spheres ( $x_p = 0.05, 0.15, 0.3,$  and  $0.6$ ) have been computed by both CEMD method and by a generalized Mie theory (GMT) [1, 36], which is an exact formulation for treating the multiple sphere problem. For both size clusters the CEMD results differ from the GMT results by at most 6%.

The agglomerates were produced by Brownian dynamics by the same method as used in Mulholland et al. [1] but starting with 16,000 primary spheres randomly located in a cubic box instead of 4000. Calculations were carried out on 28 agglomerates ranging in size from 3 spheres to 1392 spheres. The calculations were carried out for 27 orientations of the agglomerates corresponding to three values evenly distributed for each of the Euler angles. Selected calculations were performed with as many as 150 orientations. The extinction cross section was found to be relatively insensitive to the orientation whereas  $\sigma_{hh}(90^\circ)$  was found to be very sensitive to particle orientation with the standard deviation of the cross section based on the 27 orientations approximately equal to the cross section.

The calculations were carried out for 5 values of the size parameter  $x_p$  over the range from 0.05 to 0.6. This corresponds to a primary sphere diameter ranging from 10 nm to 120 nm for the case of a He-Ne laser light source at 632.8 nm. While most calculations were carried out for a refractive index of  $1.7 + i0.7$ , selected calculations were carried out for a refractive index of  $1.57 + i0.56$ , which is perhaps the

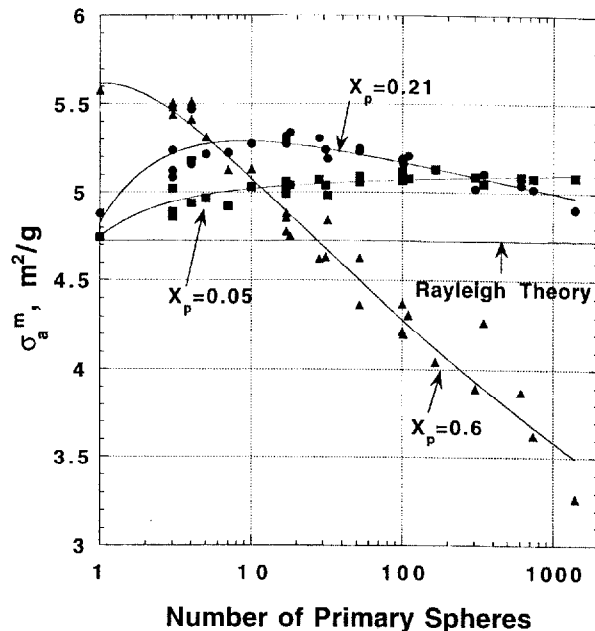


Fig. 1. The specific absorption coefficient versus number of primary spheres for  $n = 1.7 + i0.7$ . The lines are smooth fits to the computed points.

most widely used value for inferring soot volume fraction from light extinction measurements [4].

In computing the total scattering cross section, 33 angles were used in the  $\theta$  direction and 12 angles in the  $\phi$  direction. Selected calculations were carried out with as many as 297 values of  $\theta$  and as many as 48 values of  $\phi$ . The acceptance angle of the detector was assumed to be  $1^\circ$  for the calculation of the polarization ratio at  $90^\circ$ . The detection area was divided into 50 area increments in computing this ratio.

First we present the results for the total cross sections and then the polarization ratio.

## RESULTS

### Total Cross Sections

To allow comparison with measurements, the total cross section results are normalized by the agglomerate mass assuming a particle density of  $1.8 \text{ g/cm}^3$ , which is typical of measured soot densities. The value of  $\sigma_a^n$  computed based on Eq. 3 is  $4.7 \text{ m}^2/\text{g}$  relative to the range  $5.1 \text{ m}^2/\text{g}$  to  $5.6 \text{ m}^2/\text{g}$  for the peak values computed by CEMD as indicated in Fig. 1. Two reasons that

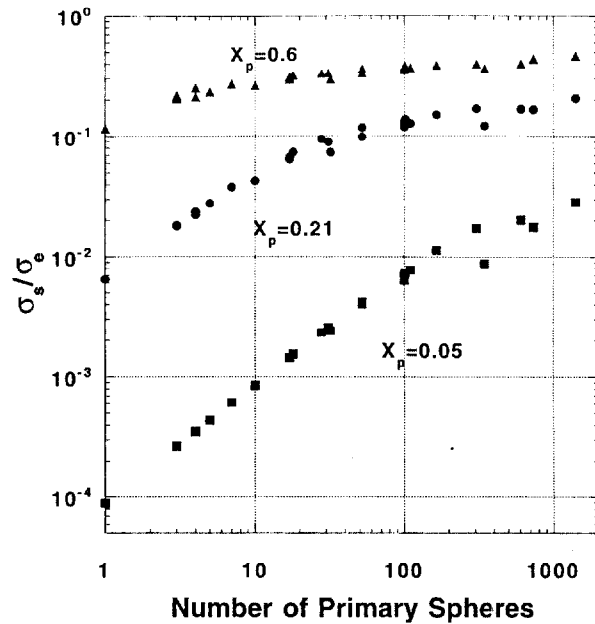


Fig. 2. The ratio of the light scattering cross section to the extinction cross section versus number of primary sphere.

Eq. 3 gives an underestimate as discussed in the Introduction are that significant deviations from the small particle limit occur for  $x_p > 0.25$  and that the coupling between the dipole fields even for very small particle sizes increases the absorption coefficient by about 10%. These effects are illustrated in Fig. 1 where the 8% and 13% increases for  $x_p$  equal 0.05 and 0.21 are primarily a result of the coupling between the dipole fields while the 17% increase for  $x_p = 0.6$  is a result of the primary sphere size being too large for Rayleigh theory to be valid. The large decrease in  $\sigma_a^m$  of about 35% for large agglomerates with  $x_p = 0.6$  is a result of screening. As discussed in the Introduction, this screening effect is apparent from the results of previous coupled dipole calculations though not at the magnitude obtained here, where we have carried out calculations for a larger size parameter and a larger agglomerate size.

As shown in Fig. 2, the ratio of the total scattering cross section to the extinction cross section for  $x_p = 0.05$  and 0.21 initially increases linearly with the number of spheres in the agglomerate, a Rayleigh-type behavior, and then appears to be approaching a constant value for larger agglomerates. For all but the largest size parameter, the contribution of the isolated scatterer is small compared to the value for an

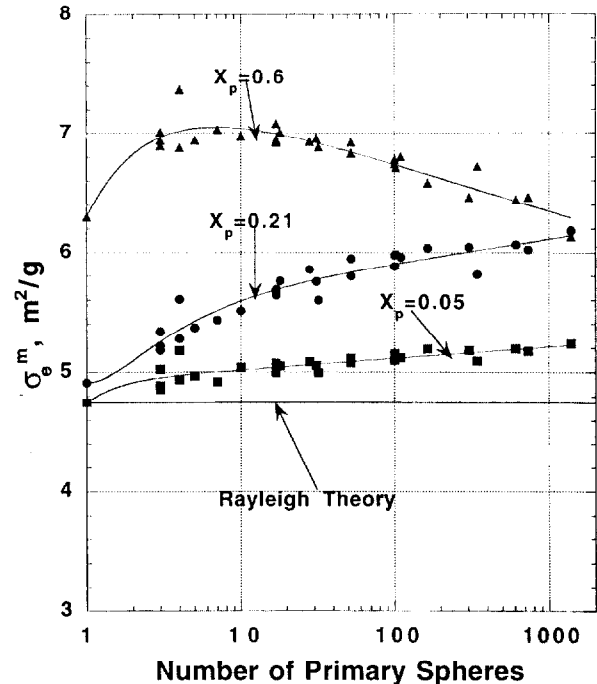


Fig. 3. The specific extinction coefficient versus number of primary spheres.

agglomerate. For the smallest primary size parameter, scattering makes a negligible contribution to the extinction cross section, at most 3%. For the parameter range relevant to laboratory-scale fires—primary spheres diameter from 30 nm to 60 nm—the maximum contribution from scattering ranges from about 18% to about 30% of the extinction cross section. This range is similar to the measured results mentioned in the Introduction [9, 26]. For the value of the size parameter characteristic of large crude oil pool fires,  $x_p = 0.6$ , the predicted scattering contribution to the extinction coefficient is about 45% for the 1392-sphere agglomerate.

The quantity of major interest experimentally is the specific extinction coefficient,  $\sigma_e^m$ , which is the sum of the absorption coefficient and the scattering coefficient. For  $x_p \leq 0.3$ ,  $\sigma_e^m$  increases with agglomerate size as a result of the increasing contribution from scattering, while for  $x_p = 0.6$  the screening effect dominates the scattering effect and  $\sigma_e^m$  decreases with increasing agglomerate size (Fig. 3). To compare with the predictions of Eq. 3, we have plotted  $\sigma_e^m$  versus agglomerate size in Fig. 4 for the size parameter range of postflame smoke corresponding to  $x_p$  values of 0.15, 0.21, and 0.30. For

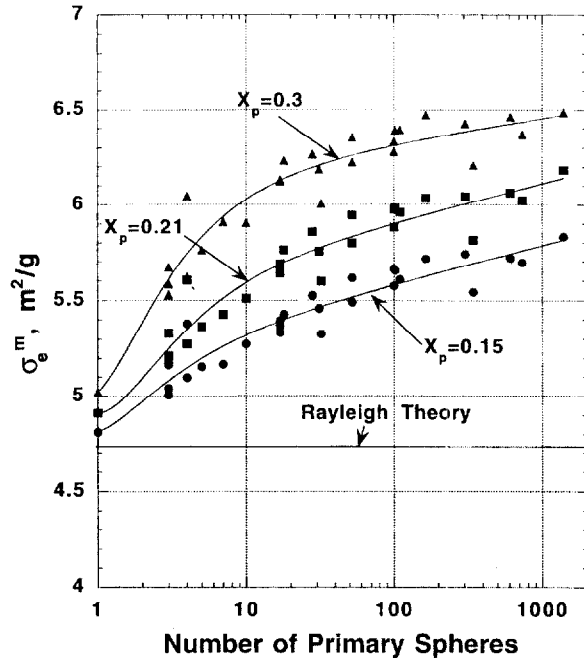


Fig. 4. The specific extinction coefficient versus number of primary spheres for a range in the primary sphere parameter,  $x_p$  from 0.15 to 0.3, encompassing most of the experimentally observed range.

cluster sizes in the range of 100–1000 primary spheres, the average value of  $\sigma_e^m$  increases from 5.7  $\text{m}^2/\text{g}$  to 6.4  $\text{m}^2/\text{g}$  as  $x_p$  increases from 0.15 to 0.3. This range in  $\sigma_e^m$  is 21% to 36% greater than the value predicted by the Rayleigh limit.

The results are sensitive to the refractive index. In Table 2 a comparison is made for the cross section obtained for a refractive index of  $1.7 + 0.7i$  and  $1.57 + 0.56i$ . The values of  $\sigma_e^m$  for the larger refractive index range from about 13% larger for  $x_p = 0.05$  to about 19% larger for  $x_p = 0.6$  than the values for the smaller refractive index. The magnitude of this refractive index effect is almost independent of agglomerate size; in fact, as indicated in Table 2, the effect for the agglomerates is similar to the

effect for a single sphere computed using Mie theory.

### Polarization Ratio

We compute the polarization ratio for a finite area detector with acceptance angle  $2\alpha$  located at a scattering angle of  $90^\circ$ . The circular detector area is divided into 50 subsectors for computing the light intensity reaching the detector. The algorithm for computing the scattered intensity for a finite acceptance angle is verified by comparison of the following analytic expression for  $r_{pol}(90^\circ)$  for Rayleigh scattering:

$$r_{pol}(90^\circ) = \frac{1}{4} \alpha^2 \quad (12)$$

The orientation averaged  $r_{pol}(90^\circ)$  for the agglomerates is determined by first computing the  $C_{hh}(90^\circ)$  and the  $C_{vv}(90^\circ)$  intensities summed over all 27 orientations and then taking the ratio. This is the appropriate method for light scattering by an ensemble of identical agglomerates in all of the 27 different orientations. Computing  $r_{pol}(90^\circ)$  for each orientation and then computing an average yields a larger value with an increase of a few percent for the smallest value of  $x_p$ , 0.05, and an increase by a factor of 2 or more for the largest value of  $x_p$ , 0.6.

The acceptance angle of the detector has a large effect on the measurement of  $r_{pol}(90^\circ)$ . The value of  $C_{hh}$  drops precipitously near  $90^\circ$  so that a slight increase in the acceptance angle produces a large increase in  $C_{hh}(90^\circ)$  averaged over the acceptance angle. As illustrated in Fig. 5 for a single sphere, the effect of acceptance angle on  $r_{pol}(90^\circ)$  is greatest for small  $x_p$ ; for example, for a size parameter of 0.15,  $r_{pol}(90^\circ)$  is seven times greater for a  $2^\circ$  ( $\alpha = 1^\circ$ ) acceptance angle relative to a  $0.6^\circ$  acceptance angle.

TABLE 2

Effect of Refractive Index on the Specific Extinction Coefficient

| # of Spheres in Agglomerate | $\sigma_e^m(n = 1.7 + i0.7)/\sigma_e^m(n = 1.57 + i0.56)$ |              |              |              |
|-----------------------------|---|--------------|--------------|--------------|
|                             | $x_p = 0.05$  | $x_p = 0.15$ | $x_p = 0.30$ | $x_p = 0.60$ |
| 1-Mie Theory                | 1.100   | 1.104        | 1.120        | 1.179        |
| 17                          | 1.124   | 1.141        | 1.176        | 1.205        |
| 52                          | 1.126   | 1.152        | 1.186        | 1.193        |
| 165                         | 1.131   | 1.158        | 1.192        | 1.183        |

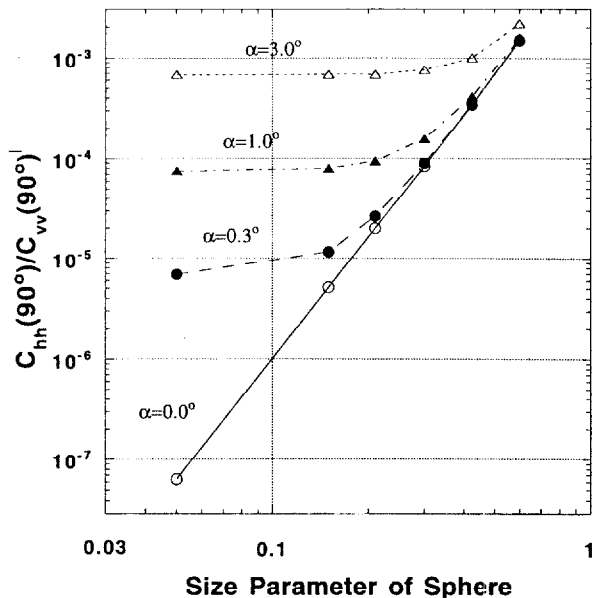


Fig. 5. The effect of the detector acceptance angle on the polarization ratio versus size parameter for spheres.

The effect of changing from an  $0.6^\circ$  to  $2^\circ$  acceptance angle is much less for agglomerates as indicated in Fig. 6 with about a 10% change at a size parameter of 0.15 and less for larger particles. The effect increases for smaller size parameters with about a 50% increase for a size parameter of 0.05 for a 165 sphere agglomerate.

The original hypothesis was that the polariza-

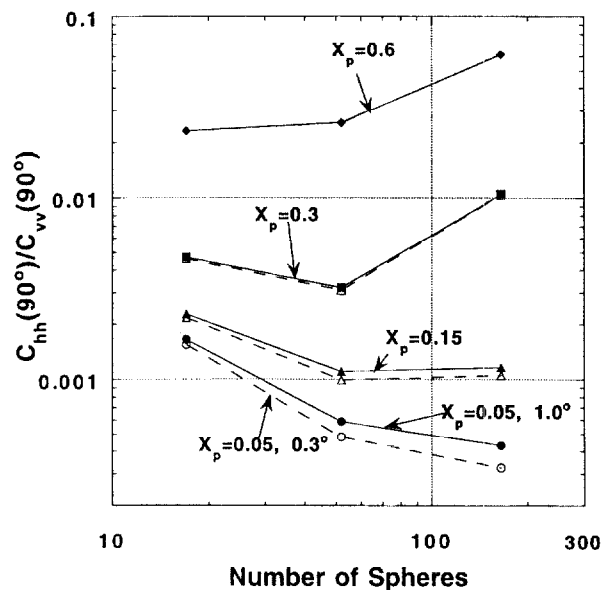


Fig. 6. The effect of acceptance angle on the polarization ratio as a function of agglomerate size and primary sphere size for a  $2^\circ$  acceptance angle.

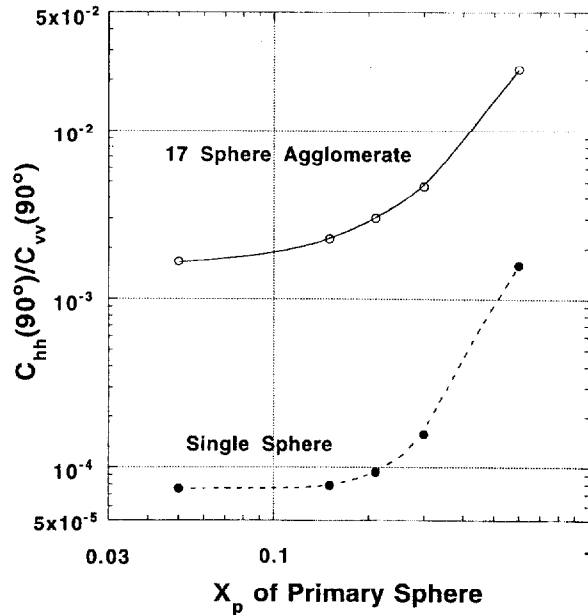


Fig. 7. Comparison of the size dependence of the polarization ratio of a single sphere and a 17-sphere agglomerate for a  $2^\circ$  acceptance angle.

tion ratio of the agglomerate would be similar to that of the primary sphere. As shown in Fig. 7 the polarization ratio is more than a factor of 10 larger than for the single sphere for a size parameter of 0.15. So this hypothesis is incorrect; the agglomerate structure does affect  $r_{pol}(90^\circ)$  through the coupled dipole fields, which may be thought of as multiple scattering within an agglomerate.

The values of the scattering cross sections at  $90^\circ$  are also very sensitive to the orientation of the agglomerate. It is found that the standard deviation of  $C_{hh}(90^\circ)$  for different orientations is comparable to the value itself for all primary sphere sizes. The large value of the standard deviation is thought to be a result of the changes in the coupled dipole fields arising from different orientations together with the small magnitude of  $C_{hh}(90^\circ)$ . For small clusters with small primary sphere sizes,  $C_{vv}(\theta)$  is Rayleigh-like with intensity proportional to the square of the number of primary spheres and is relatively independent of angle. In this regime the orientation has a relatively small effect on the scattering and the standard deviation is on the order of 10% to 20% of the mean value. However, for large agglomerates and/or large primary spheres the standard deviation for  $C_{vv}(90^\circ)$  approaches the size of the mean value.

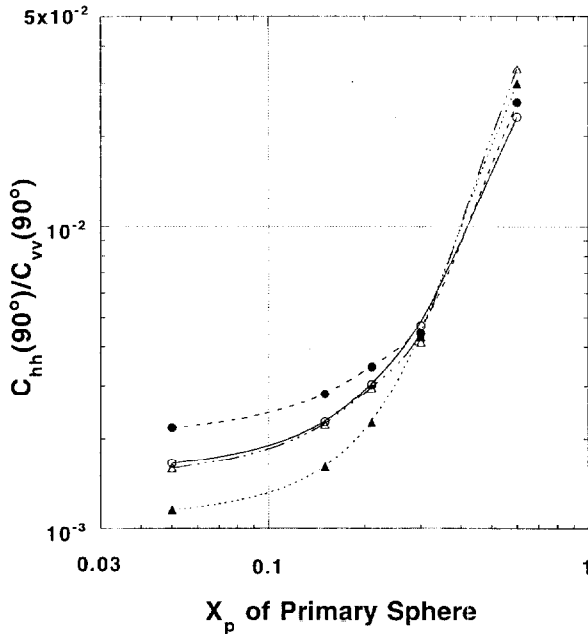


Fig. 8. Polarization ratio versus size parameter for 4 different 17-sphere agglomerates for a  $2^\circ$  acceptance angle.

The number of orientations was increased to 180 for the three 17-sphere agglomerates and to 216 for the 28 sphere agglomerate. The results were affected by 10% or less except for the largest size parameter for one of the agglomerates. We see that scattering at a specific angle is sensitive to the orientation and that 27 orientations are adequate for obtaining a representative average. For total scattering cross section and for the extinction cross section the effect of orientation is relatively small with a standard deviation equal to a few percent of the mean.

Even for clusters with the same number of primary spheres, there are differences in  $r_{pol}(90^\circ)$ ; for example, there is a factor of 2 difference in  $r_{pol}(90^\circ)$  for 3 17-sphere agglomerates for small  $x_p$  as shown in Fig. 8. Results for larger agglomerates with up to 346 spheres given in Fig. 9 also illustrate this effect of the detailed structure of the agglomerate; however, for these agglomerates as well as the 17-sphere agglomerate, the effect of primary sphere size is much greater than is the effect of the detailed structure of the agglomerate.

The effect of the number of primary spheres on  $r_{pol}(90^\circ)$  is summarized in Fig. 10. The ratio appears to be independent of agglomerate size for  $x_p$  equal 0.21, there is a slight increase for  $x_p$  equal 0.6, and a large decrease for  $x_p$  equal 0.05

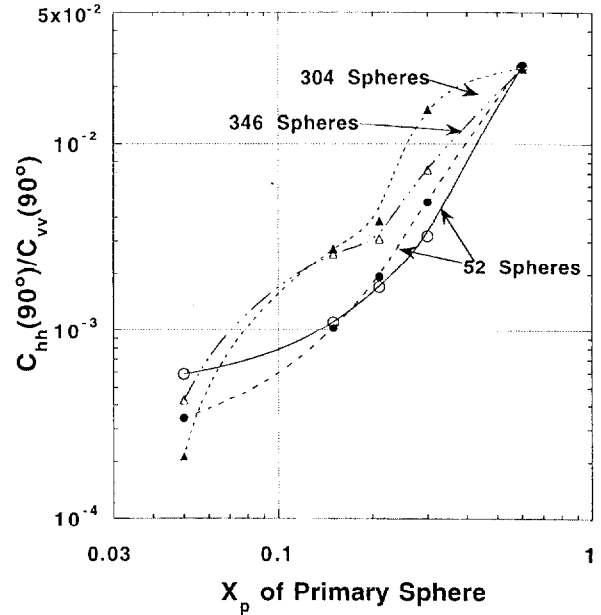


Fig. 9. Polarization ratio versus primary sphere size for agglomerates with 52, 304, and 346 spheres.

though in all cases there is large variability resulting from the detailed structure of the agglomerate. This variability is not a result of the calculation. The estimated effects of the finite number of orientations (27) and the finite number of scattering subsectors (50) is less than 10%.

Most postflame smokes have agglomerates

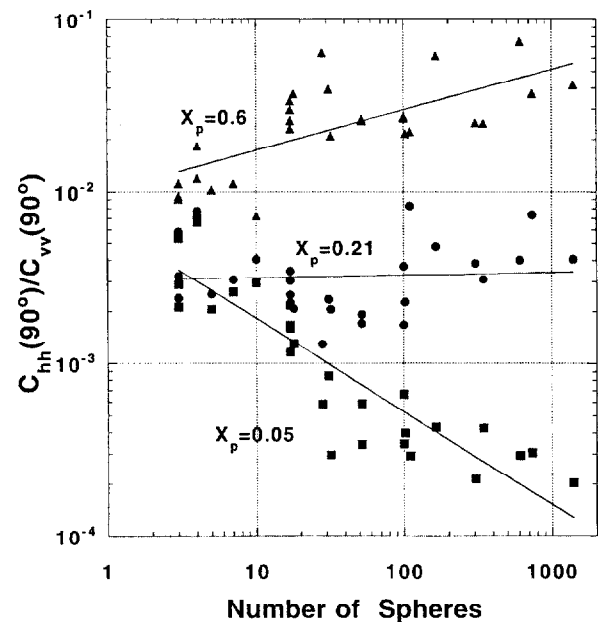


Fig. 10. Summary plot of the effects of both size parameter and number of spheres in the agglomerate on the polarization ratio for a  $2^\circ$  acceptance angle.

with more than 100 primary spheres [13]. The effect of agglomerate size on  $r_{pol}(90^\circ)$  is relatively small, at most about a factor of 2, for fixed primary sphere size for agglomerates with more than 100 spheres. On the other hand, the average value of  $r_{pol}(90^\circ)$  is very sensitive to primary sphere size increasing by almost a factor of 100, from  $3.7 \times 10^{-4}$  to  $3.6 \times 10^{-2}$  as  $x_p$  increases by a factor of 12 from 0.05 to 0.6.

For actual smoke there is a population of many different cluster sizes. Koylu and Faeth [13] find that the smoke agglomerate distribution for eight hydrocarbon fuels has a log-normal distribution with a geometric mean cluster size ranging from 160 to 290 and a geometric standard deviation of about 3. We have computed the polarization ratio summed over all the clusters and 27 different orientations for each cluster where we have weighted the contribution for each cluster size based on a log-normal size distribution,  $f(N_i)$ , with geometric standard deviation equal 3 and geometric mean number sizes of 30 and 300.

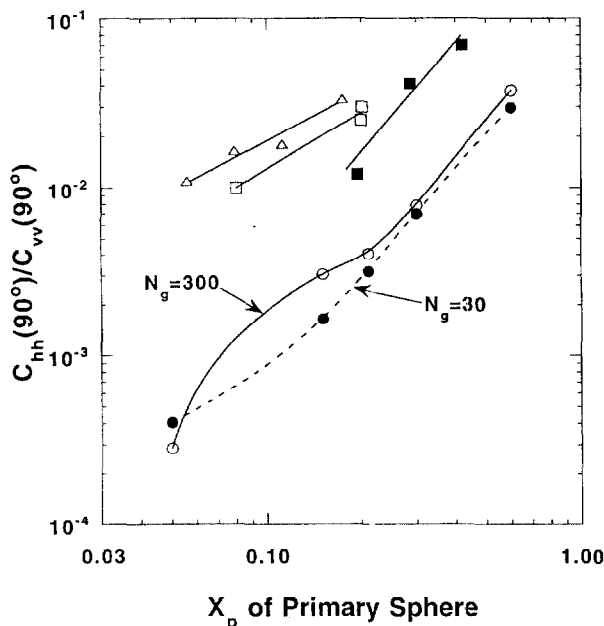


Fig. 11. Polarization ratio versus size parameter for a log normal distribution of agglomerate size for geometric mean cluster number of 30 and 300 for a geometric standard deviation of 3.0. The experimental data includes laminar ethane burner (open squares) [29, 37], laminar methane burner—steady and pulsed (open triangles) [10, 40], and turbulent acetylene flame (closed squares) [38].

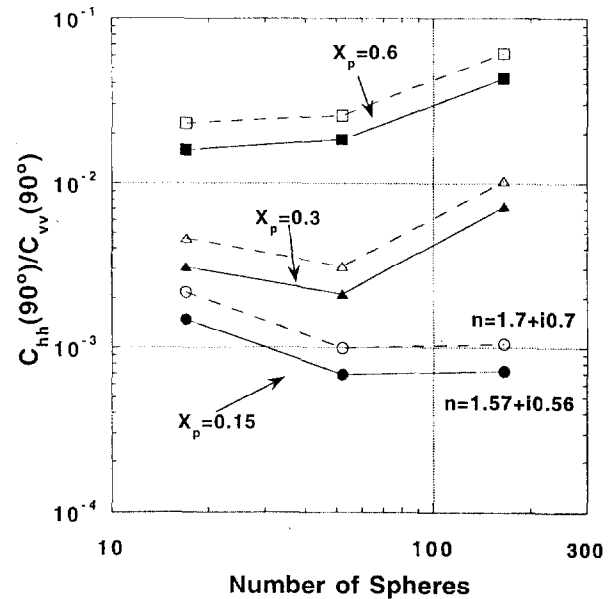


Fig. 12. The effect of refractive index on the polarization ratio.

$$\frac{C_{hh}(90^\circ)}{C_{vv}(90^\circ)} = \frac{\sum_i \sum_j C_{hh}^{ij}(90^\circ) f(N_i)}{\sum_i \sum_j C_{vv}^{ij}(90^\circ) f(N_i)} \quad (13)$$

This averaged result mimics experiment where hundreds or thousands of agglomerates are present in the scattering volume and significant agglomerate rotation takes place over the measurement time. It is seen in Fig. 11 that there is almost a two order of magnitude increase in  $r_{pol}(90^\circ)$  with increasing primary sphere size. Comparison with experimental results will be discussed in the next section.

All of the calculations to this point have assumed a refractive index equal  $1.7 + i0.7$ . As discussed in the Introduction, there is a large uncertainty in the value of refractive index. Figure 12 illustrates that changing the refractive index to  $1.57 + i0.56$  results in about a 40% reduction in  $r_{pol}(90^\circ)$ , which is approximately equal to the reduction in the value based on Mie theory analysis for a single sphere.

## DISCUSSION

### Specific Extinction Coefficient

The calculated value of  $\sigma_e^m$  is in the range of 5.6 to 6.4  $m^2/g$  for agglomerates ranging in size

from 100 to 1392 primary spheres and size parameters in the range 0.15 to 0.3. This suggests that even if the refractive index of all smokes were identical there would still be on the order of a 10 to 15% range in the specific extinction coefficient because of the range in primary sphere sizes and agglomerate sizes.

The calculated range of 5.6 to 6.4 m<sup>2</sup>/g differs significantly from the measured values in the range 7.5 to 9.5 m<sup>2</sup>/g. Why the difference? We believe that the major reason for the difference is that the refractive index of smoke is not 1.7 + *i*0.7. As discussed above the value of  $\sigma_e^m$  is sensitive to the refractive index. By changing the refractive index from 1.7 + *i*0.7 to 1.57 + *i*0.56, the value  $\sigma_e^m$  decreases by 20% for a 165-sphere agglomerate for size parameter of 0.3. As indicated in Table 1, there is a wide range of reported values for the refractive index of flame-generated smoke. The uncertainties in the measurements are difficult to assess because of the agglomerate structure of the particles. Even for widely used reflectance measurements from a compressed pellet of smoke agglomerates, a validated model for inferring refractive index from the reflectance measurements does not exist. Of all the values in Table 1, the one with the largest imaginary component,  $n = 1.7 + i0.8$ , yields the largest specific extinction coefficient in the Rayleigh limit, which is 12% larger than for a refractive index of 1.7 + *i*0.7. The estimated value of  $\sigma_e^m$  for an agglomerate of 1392 spheres and  $x_p = 0.21$  with these optical properties is 6.9 m<sup>2</sup>/g, which is near the low end of the measured values. For refractive index of 1.55 + *i*0.8, which is outside the range of values given in Table 1, the estimated value of  $\sigma_e^m$  for these same conditions is 8.0 m<sup>2</sup>/g, which is in the middle of the experimental range. Dobbins et al. [4] obtained a similar value, 7.8 m<sup>2</sup>/g for  $n = 1.55 + i0.78$ , based on an approximate fractal optics model assuming the large agglomerate limit for scattering and including a second-order correction in computing the specific absorption of the 45-nm-diameter primary spheres.

As pointed out by Dobbins et al. [4], the values of the refractive index that give agreement are not uniquely determined by solely matching the specific extinction coefficient. Equally good agreement would be obtained for

a larger value of the real part of the refractive index if the imaginary part were also increased by the appropriate amount. The point is that none of the values of the refractive index given in Table 1 are consistent with the measured specific extinction coefficient. The predicted specific extinction coefficients based on these values are all smaller than the measured values.

There are two other differences between the current model calculations and actual postflame smoke. For some hydrocarbons including acetylene and aromatics, flaming combustion typically produces agglomerates with as many as 10<sup>4</sup> to 10<sup>6</sup> primary spheres. Calculations for larger agglomerates are needed to determine whether  $\sigma_e^m$  approaches an asymptotic value with increasing agglomerate size or whether it changes. Secondly, for actual smoke the "touching" spheres are in some cases partially fused (i.e., necks between primaries). This necking is not expected to be a major factor for carbonaceous particles, which have a relatively low conductivity, but model calculations are needed to quantify this effect for both the light extinction properties and for the polarization ratio discussed below. For highly conducting particles like gold and silver this necking effect is expected to be more significant.

As discussed in the Introduction, there is also a need for additional experimental study to resolve why the results from the turbulent diffusion burning of gaseous hydrocarbon fuels at an intermediate scale, 3–20 kW, [9] are significantly different from results for gaseous and liquid hydrocarbon fuels along with plastics, wood, and various petroleum distillate fractions obtained over a range of fire scales [5–8].

### Polarization Ratio

There are several flames where both polarization ratio and primary sphere size have been measured. In-flame measurements of the polarization ratio for a laminar ethene flame were made by Dobbins et al. [29] using an Ar-ion laser and photomultiplier detection; thermophoretic sampling and transmission electron microscopy (TEM) analysis of the soot were carried out for the same flame system by Megaridis and Dobbins [37] (Fig. 11, open squares). Faeth and Koylu [38] used a similar

method for characterizing postflame soot agglomerates produced by buoyant turbulent flames produced by eight hydrocarbon fuels with results for ethene and acetylene included in Fig. 11 (closed squares). Measurements were performed at both the Ar-ion laser wavelength of 514 nm as well as 351 nm [39]. Shaddix et al. [40] produced a sheet of light with a pulsed laser and used charge-coupled device (CCD) detection so that measurements could be made over an extended region for both a steady and flickering methane flame. The polarization ratios in Fig. 11 (open triangles, Shaddix, personal communication) are for heights of 50, 60, and 70 mm for the steady flame and 90 mm for the flickering flame. Megaridis and Zhang [10] applied a phase-locked thermophoretic sampling probe for collecting and sizing the primary sphere size for this same flame system.

The in-flame measurements show a trend of increasing  $r_{pol}(90^\circ)$  with increasing size parameter as does the model calculation. We believe this similarity in trend points to the potential utility of polarization ratio measurements as a diagnostic tool for monitoring the primary sphere size of agglomerates in flame environments.

While the trends are similar, the measured  $r_{pol}(90^\circ)$  is a factor of 5–10 larger than the model prediction. Possible reasons for this difference are discussed below. First, the sizes measured by electron microscopy are based on the number average size; however, Rayleigh scattering is related to the 6th moment of the size distribution for the primary spheres. So the light scattering weighted size will be larger than the number average size obtained by electron microscopy resulting in a shift of the experimental data in Fig. 11 toward larger  $x_p$ . Second, the calculations assume that only light with scattering angles between  $89^\circ$  and  $91^\circ$  and with a solid angle of  $1.0 \times 10^{-3}$  sr reach the detector. The acceptance angle for the two studies using photomultiplier tubes had a similar solid angle of  $1.2 \times 10^{-3}$  sr, while the third study with a CCD array had a larger acceptance angle and a larger scattering volume. So it is not surprising that the results would differ for this case. Third, if the primary particles are aspherical, there will be a contribution to  $r_{pol}(90^\circ)$  not accounted for in the CEMD model. For small spheroids,

$r_{pol}(90^\circ)$  is dependent on the aspect ratio of the particle and independent of the particle volume [41]. Fourth the “necking between primary spheres” observed in actual soot may impact the value of the polarization ratio.

The experimental status should be viewed as a helpful first glimpse but not definitive. None of the papers referenced above focused on the polarization ratio measurements and the measurement uncertainties for  $r_{pol}(90^\circ)$  are not discussed. One promising application of this method would be as a diagnostic for relative changes in primary particle size for one fuel as the sampling location is varied as well as the combustion conditions.

Quantitative measurements and calculations of  $r_{pol}(90^\circ)$  are needed for agglomerates made up of monodisperse spheres, “necking spheres,” and spheroids with well-defined aspect ratio to determine the significance of the primary particle diameter effect relative to the shape effect. Also as discussed above, the large dependence of the polarization ratio on the detailed structure of the agglomerate suggests that future studies should include a larger number of agglomerates, ideally 100 per decade, and include larger agglomerate sizes up to  $10^4$  to  $10^5$  primary spheres.

## CONCLUSIONS

1. Rayleigh theory underestimates the specific extinction coefficient by 21% to 36% relative to CEMD model for agglomerates with 100–1000 primary spheres for primary sphere size parameter in the range 0.15 to 0.30.
2. For a fixed refractive index, there is a 10% to 15% range in the specific extinction coefficient of smoke ( $5.6 \text{ m}^2/\text{g}$  to  $6.4 \text{ m}^2/\text{g}$ ) for agglomerates with 100 to 1392 primary spheres and size parameters in the range 0.15 to 0.3.
3. For the literature values for the refractive index of soot, the computed specific extinction coefficient is smaller than most of the measured values; for a refractive index of  $1.55 + i0.8$  the CEMD values agree with the measured values.
4. The specific absorption coefficient decreases for large agglomerates for primary size parameter of 0.21 and larger. For a primary size

parameter of 0.6, the coefficient decreases by 35% as agglomerate size increases from 3 to 1000 primary spheres.

- CEMD calculations indicate that polarization ratio measurements at 90° has good potential as a diagnostic for the primary sphere size in a flame.

## REFERENCES

- Mulholland, G. W., Bohren, C. F., and Fuller, K. A., *Langmuir* 10:2533 (1994).
- Choi, M. Y., Mulholland, G. W., Hamins, A., and Kashiwagi, T., *Combust. Flame* 102:161 (1995).
- Dobbins, R. A., Mulholland, G. W., and Bryner, N. P., *Atmos. Environ.* 28:889 (1994).
- Smyth, K. C., and Shaddix, C. R., *Combust. Flame* 107:314 (1996).
- Choi, M. Y., Mulholland, G. W., Hamins, A., and Kashiwagi, T., *Combust. Flame* 102:161 (1995).
- Patterson, E. M., Duckworth, R. M., Wyman, C. M., Powell, E. A., and Gooch, J. W., *Atmos. Environ.* 25:2539 (1991).
- Dobbins, R. A., Mulholland, G. W., and Bryner, N. P., *Atmospheric Environment* 28:889 (1994).
- Mulholland, G. W., Henzel, V., and Babrauskas, V., in *Proceedings of the Second Fire Safety Science International Symposium* (T. Wakamatsu, Y. Hasemi, A. Sekizawa, P. G. Seeger, P. J. Pagni, and C. E. Grant, Eds.) Hemisphere, New York, 1989, p. 347.
- Wu, J.-S., Krishnan, S. K., and Faeth, G. M., *J. Heat Transfer* 119:230 (1997).
- Zhang, J., and Megaridis, C. M., *Combust. Flame* 112:473 (1997).
- Dobbins, R. A., and Megaridis, C. M., *Langmuir* 3:254 (1987).
- Samson, R. J., Mulholland, G. W., and Gentry, J. W., *Langmuir* 3:272 (1987).
- Koylu, U. O., and Faeth, G. M., *Combust. Flame* 89:140 (1992).
- Mulholland, G. W., Koscki, H., and Liggett, W., *Twenty-Sixth Symposium (International) on Combustion*, The Combustion Institute, Pittsburgh, 1996, p. 1445.
- Pluchino, A. B., Goldberg, S. S., Dowling, J. M., and Randall, C. M., *Appl. Optics* 19:3370 (1980).
- Dalzell, W. H., and Sarofim, A. F., *J. Heat Transfer* 91:100 (1969).
- Lee, S. C., and Tien, C. L., *Eighteenth Symposium (International) on Combustion*, The Combustion Institute, Pittsburgh, 1981, p. 1159.
- Sloane, C. G., *Atmos. Environ.* 17:409 (1983).
- Mullins, J., and Williams, A., *Fuel* 66:277 (1987).
- Chang, H., and Charalampopoulos, T. T., *Proc. R. Soc. Lond. A* 430:577 (1990).
- Stagg, B. J., and Charalampopoulos, T. T., *Combust. Flame* 94:381 (1993).
- Nelson, J., *J. Mod. Opt.* 36:1031 (1989).
- Iskander, M. F., Chen, H. Y., and Penner, J. E., *Atmos. Environ.* 25A:2563 (1991).
- Farias, T. L., Carvalho, M. G., Koylu, U. O., and Faeth, G. M., *Trans ASME* 117:152 (1995).
- Sorensen, C. M. (1996). *Post-Flame Soot*. NIST-GCR-96-694, National Institute of Standards and Technology, Gaithersburg, MD.
- Patterson, E. M., Duckworth, R. M., Wyman, C. M., Powell, E. A., and Gooch, J. W., *Atmos. Environ.* 25:2539 (1991).
- Kerker, M., *The Scattering of Light and Other Electromagnetic Radiation*, Academic Press, New York, 1969.
- D'Slessio, A., in *Particulate Carbon Formation During Combustion* (D. C. Siegla and G. W. Smith, Eds.) Plenum Press, New York, 1981, p. 207.
- Dobbins, R. A., Santoro, R. J., and Semerjian, H. G., in *Combustion Diagnostics by Nonintrusive Methods* (T. D. McCay and J. A. Roux, Eds.), *Progress in Astronautics and Aeronautics*, American Institute of Aeronautics and Astronautics, 1984, 92:208.
- Jones, A., *Proc. R. Soc. Lond. A* 366:111 (1979).
- Mountain, R. D., and Mulholland, G. W. *Langmuir* 4:1321 (1988).
- Sorensen, C. M., Cai, J., and Lu, N., *Appl. Opt.* 31:6547 (1992).
- Bohren, C. F., and Huffman, D. R., *Absorption and Scattering of Light by Small Particles*, John Wiley, New York, 1983, p. 101.
- Purcell, E. M., and Pennypacker, C. R., *Astrophys. J.* 186:705 (1973).
- Dungey, C. E., and Bohren, C. F., *J. Opt. Soc. Am. A: Opt. Image Sci.* 8:81 (1991).
- Michel, B., Henning, T., Stognienko, R., and Rouleau, F., *Astrophys. J.* 468:834 (1996).
- Megaridis, C. M., and Dobbins, R. A., *Combust. Sci. Technol.* 66:1 (1989).
- Faeth, G. M., and Koylu, U. O. *Combust. Sci. Technol.* 108:207 (1995).
- Wu, J. S., Krishnan, S. K., and Faeth, G. M., *J. Heat Transfer* 119:230 (1997).
- Shaddix, C. R., Harrington, J. E., and Smyth, K. C., *Combust. Flame* 99:723 (1994).
- Van de Hulst, H. C., *Light Scattering by Small Particles*, Dover, New York, 1981, p. 70.

Received 16 April 1998; revised 4 January 1999; accepted 4 March 1999